Article no. 25

THE CIVIL ENGINEERING JOURNAL 4-2016

NUMERICAL ANALYSIS OF THE EFFECT OF SURCHARGE ON THE MECHANICAL BEHAVIOR OF GEOCELL REINFORCED RETAINING WALL

Fei Song[1], Haibo Chai[1], Jian Zhao[2], Mingrui Yang[2]

1 Institute of Geotechnical Engineering School of Highway Engineering, Chang'An University, Xi'an, 710064, P.R.China; E-mail: songf1980@163.com

2 Guizhou Electric Power Design Institute and Research Institute, Guiyang, 550002, P.R. China

ABSTRACT

Geocell reinforced retaining structure has been widely used in civil engineering for the protection of slopes due to its advantages. In this paper, the effects of surcharge on the horizontal displacement of the wall back, the size of the sliding wedge and the factor of safety of geocell reinforced retaining wall are numerically analyzed by employing the geotechnical finite element method software Plaxis. The research results show that, when the distance of surcharge from the wall face is small, the maximum and the minimum deformation of the wall back takes place near the top of the wall and the wall bottom respectively. After the distance of surcharge from the wall face exceeds about 13% of the wall height, the surcharge has little effect on the horizontal deformation of the wall back, the size of the sliding wedge and the safety factor of geocell reinforced retaining wall. The horizontal deformation of the wall back gradually increases with the increase of the length of the surcharge until it reaches a certain value. The effect of the length of the surcharge on the failure surface is not significant. Besides, the factor of safety of the wall gradually decreases with the increase of length of the surcharge. However, with the increase of the distance of the surcharge from the wall face, the influence of the length of the surcharge on the safety factor gradually becomes small. The study results can supplement theoretical basis for the design of geocell reinforced retaining walls in engineering practices.

KEYWORDS

Geocell reinforced retaining wall, surcharge, sliding wedge, horizontal displacement, safety factor

INTRODUCTION

Geosynthetics are widely used as reinforcing members in the construction of earth structures due to its superior properties compared with other materials, such as those of Zigler and and Pokorný (2005) [1], Liu (2016) [2]. In recent years, the use of geosynthetic materials for reinforced slopes and retaining walls has increased significantly throughout the world because of the increasing infrastructural development demands. A lot of research efforts have been made to study geosynthetic-reinforced soil structure.

Leshchinsky (1989) conducted a limit equilibrium analysis for the internal stability of geosynthe-reinforced vertical walls and studied the influences of two possible extreme inclinations of the reinforcement's tensile resistance [3]. Wong and Broms (1994) conducted a series of model tests to study the failure modes of a geotextile-reinforced soil wall [4]. Porbaha and Goodings (1996) studied the effect of the foundation soil, the slope inclination angle and the geotextile strengths on the reinforced wall behavior by centrifuge model tests of twenty-four models of geotextile-reinforced cohesive-backfill retaining walls [5]. Rowe and Skinner (2001) performed a numerical examination of the behavior of an 8 m high geosynthetic reinforced soil wall constructed on a layered foundation stratum [6]. Koerner and Soong (2001) presented the evolution and a cost survey of geosynthetic reinforced segmental retaining walls in general [7]. They also compared three design methods in detail. Yoo (2004) explored the possible causes of distress and unexpected large lateral wall movements of a 6-year-old geosynthetic-reinforced segmental retaining wall and recommended several remedial measures [8]. Hatami and Bathurst (2005) developed a numerical model to simulate full-scale, geosynthetic-reinforced soil walls under working stress conditions [9]. Bathurst et al. (2006) investigated the influence of facing type and stiffness on the reinforcement loads by the measurements of two instrumented full-scale walls with different facing stiffness [10]. Benjamim et al. (2007) measured the internal distribution of reinforcement strains, the overall vertical and horizontal movements within the reinforced soil mass, as well as face displacements by field monitoring a geotextile-reinforced soil-retaining prototype wall [11]. Won and Kim (2007) measured local deformation of geosynthetics, such as geogrids, and nonwoven and woven geotextiles, to analyze the stability of geosynthetic-reinforced soil (GRS) structures [12]. Sabermahani et al. (2009) studied the seismic deformation modes of reinforced-soil walls by conducting a series of 1-g shaking table tests on 1 m high reinforced-soil wall models [13]. Bathurst et al. (2009) studied the influence of reinforcement stiffness and compaction method on wall displacement by field monitoring four geosynthetic-reinforced soil walls [14]. Leshchinsky (2009) established a benchmark test and examined the validity of the three existing design methods in the United States [15]. Ehrlich et al. (2012) performed a physical model study of the influence of compaction on the behavior of geogrid-reinforced soil walls [16]. Suksiripattanapong et al. (2012) performed a numerical analysis of the bearing reinforcement earth wall by PLAXIS 2D [17]. Liu (2012) estimated the lateral facing displacement at the end of construction as well as after years of creep of geosynthetic-reinforced soil segmental retaining walls by FEM analysis [18].

Although considerable interest has been shown in reinforced walls, little has been published concerning geocell retaining structures, shown in *Figure 1*. Due to its unique three-dimensional geometry, geocell can provide great lateral confinement to the infill soil without relying on the interlocking or friction with the infill soil. The geocell reinforced retaining structures have been used extensively in embankment and slope protection due to the advantages of simple installation, cost-effectiveness and ecological protection. Xie and Yang (2009) studied the deformation and mechanical properties of geocell retaining walls by the FEM numerical simulation [19]. Chen and Chiu (2008) performed on nine model geocell retaining walls and examined the facing displacement and settlement of backfill [20]. Song et al. (2011) analyzed the effects of the aspect ratio, slope inclination angle and surcharges on the deformation behavior of the geocell retaining wall by the numerical analysis [21]. Chen et al. (2013) assessed the stability and deformation of geocell structures with various layouts by numerical analysis [22]. Song et al. (2013a) investigated the failure process of the geocell reinforced retaining wall with surcharge acting on the backfill surface by means of the centrifugal model tests [23]. Song et al. (2013b) studied the effects of soil strength and the strength of geocell structure on the failure surface of geocell reinforced retaining wall by numerical simulation [24]. Song et al. (2014a) performed a series of centrifuge model tests on geocell reinforced retaining wall to study the effect of aspect ratio and the slope inclination on

the failure surface. In addition, they compared measured failure surfaces with those predicted by Coulomb and Rankine's earth pressure theories and revealed the differences [25]. Song et al. (2014b) studied the optimum sectional form of the geocell reinforced retaining wall by numerical analysis [26]. Song et al. (2014c) formulated mathematical expression of the failure surfaces of geocell reinforced retaining walls with different height-width ratios and backfill strengths [27]. However, the mechanical behavior of geocell reinforced retaining walls with surcharge acting on is not systematically investigated.

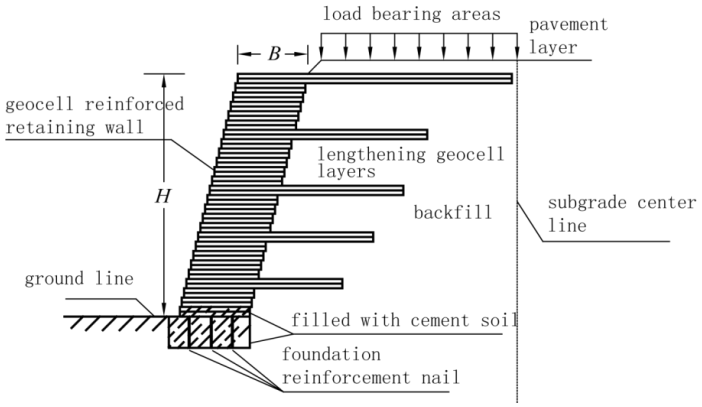

(a) Schematic diagram of geocell reinforced retaining wall

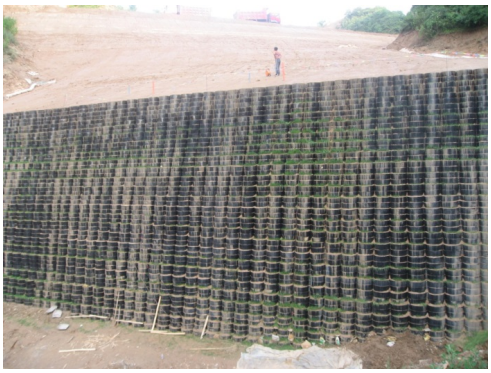

(b) Photo of geocell reinforced retaining wall

Figure 1 - Geocell reinforced retaining structures used for embankment protection

In this paper, by employing the geotechnical finite element method software Plaxis, the numerical models of geocell reinforced retaining walls with surcharge acting on are formulated and the mechanical behavior of the wall is studied by numerical simulation. On the basis of analysis of the numerical simulation results, the effects of the distance of the surcharge from the wall face and the length of the surcharge on the horizontal displacement, the sliding surface and the safety factor of the wall are investigated. The research results provide theoretical basis and references for the design of the wall.

Model and parameters of calculation

By employing the geotechnical finite element method software Plaxis, the mechanical behavior of a geocell reinforced retaining wall with surcharge acting on is numerically simulated in order to study the effect of the surcharge on the horizontal deformation, the failure surface and the

safety factor on the wall. In this study, the geocell reinforced soil is treated as a composite material with addition cohesive strength and siffness resulted from the confinment effect. Because of its convenience and simplication, such 2-dimensional equalient model has been employed and its effectiveness has been validated by Mhaiskar and Mandal (1996) [27], Bathurst and Knight (1998) [28], Latha (2000) [29], Rajagopal et al. (2001) [30], Latha et al. (2006) [31], Latha and Rajagopal (2007) [32], Latha et al. (2008) [33], Xie and Yang et al. (2009) [19], Latha et al. (2009) [34], Chen et al. (2013) [22], Mehdipour et al. (2013) [35]. In the computation, the 15-node triangular element is employed in this analysis to model soil, the geocell reinforced soil and the foundation. An elastic-plastic model employing the Mohr-Coulomb criterion is adopted for the backfill, the geocell reinforced soil and the foundation. In addition, the interface element is set between each geocell structure layer, between the wall back and backfill, and also between the foundation and the soil to model the interaction between the structure and the soil. Phi-c reduction in Plaxis is employed to calculate failure surfaces and safety factors of the wall. The details of constitutive model of the materials, the interface element, the phi-c reduction method and the definition of safety factor in Plaxis can be referred to Brinkgreve and Broere (2000) [36], Song et al. (2013b) [24].

With references to calculation parameters adopted by Wang (2004) [37], Xie and Yang (2009) [19], based on the analysis of the mechanical property tests of geocell by Yang (2005) [38], the mechanical parameters of the wall body, the foundation and the backfill in this study are selected and listed in Table 1. In order to be conservative, the magnitudes of the strength and modus of the geocell wall body are a little smaller than the ones previously adopted.

Table 1 - Calculation Parameters of Model

Material	Wall Body	Foundation	Backfill
γ/(kN/m^3)	18	20	17
γ_{sat}/(kN/m^3)	20.5	22	20
c/kPa	45	70	30
φ/(°)	30	45	25
E/MPa	50	65	30
v	0.25	0.2	0.35
R_{inter}	0.67	0.67	0.67

The calculation model illustrated in *Figure 2* is composed of the geocell structure layers, the foundation and the backfill. *a* and *b* in *Figure 2* represent respectively the distance of the surcharge from the face and the length of the surcharge. In the computation, the height of the geocell reinforced retaining wall is 10m, the width of the wall is 4m and the slope ratio is 1:0.25. In addition, the height of each geocell layer is 40cm. The geocell reinforced retaining wall and the foundations are built by stage construction in nine steps. The foundation is constructed in the first step and the embankment and geocell reinforced retaining wall are filled by 2m/d in the following eight steps. As is shown in *Figure 2*, ten representative points are selected along the wall back in order to study the horizontal deformation of the wall in different conditions. If the wall toe is selected as coordinate origin, the coordinates of the ten points from the wall top to the wall bottom are respectively A(6.5, 10.0), B(6.3, 9.0), C(6.0, 8.0), D(5.7, 7.0), E(5.5, 6.0), F(5.2, 5.0), G(5.0, 4.0), H(4.7, 3.0), I(4.4, 1.5), J(4, 0). After the construction is finished, surcharge is exerted on the backfill surface and the horizontal deformation is predicted by a plastic calculation. After that, the failure surface and the factor of safety are calculated by the strength reduction method built in Plaxis.

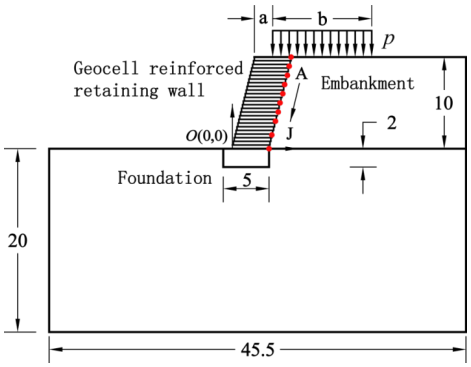

Figure 2 - Sketch of the calculation model (Unit: m)

EFFECT OF DISTANCE OF SURCHARGE FROM THE WALL FACE

The initial stress field is produced by K_0 procedure in Plaxis. The deformation caused by the initial stress has no actual physical meanings and is therefore removed in the first step of the calculation, which can eliminate the effect of the deformation induced by the initial stress on the successive stress and displacement field. In the successive analysis, *p* and *H* represent the magnitude of the surcharge and the wall height respectively. In the computation, *b*=5m, i.e. *b*/*H*=0.5, and only the value of *a* is changed. In some cases, for example, when *a*/*H*=0.1～0.4, *p*=150kPa, the soil body collapses and the calculation cannot be completed. The horizontal deformation of the wall back with different *a*/*H* values is shown in *Figure 3*. The case of the wall without surcharge acting on is superimposed in the figure for comparison.

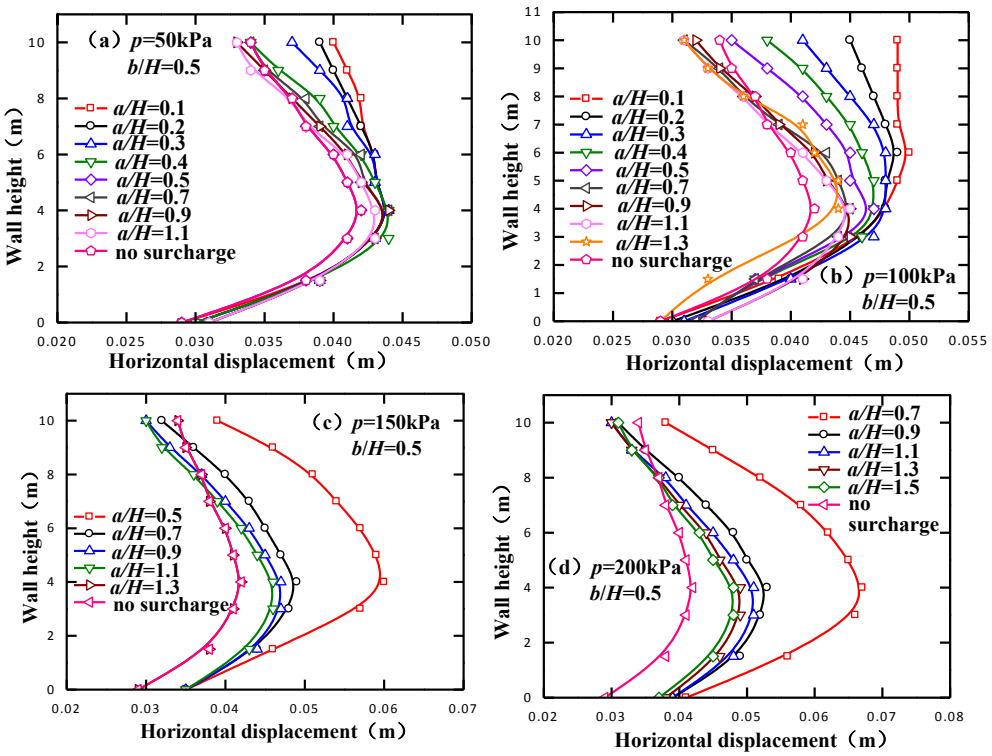

Figure 3 - Effect of distance of surcharge from wall face on the horizontal deformation (Unit: m)

It can be observed from *Figure 3* that when the surcharge is near the wall face, the maximum deformation of wall back takes place near the top of the wall for the cases of *p*=100kPa and the difference between the horizontal deformation of the top of the wall and that at about *H*/3 above the wall heel is relatively small for the cases of *p*=50kPa. For the case of *p*=100kPa, with the increase of the distance of the surcharge from the wall face, the location where the maximum deformation of wall back occurs gradually descends and the shape of the curve representing the deformation of the wall back changes. For all the cases, with the increase of the distance of the surcharge from the wall face, the horizontal displacement gradually decreases and the shape of the curve becomes the one with the largest horizontal deformation at location about *H*/3 above the wall heel, from which the horizontal deformation gradually decreases toward the wall top and wall heel respectively, which is the same case with the wall without surcharge revealed by the previous studies of Song et al. (2011). This indicates that with the increase of the distance of the surcharge from the wall face, the effect of the surcharge on the horizontal displacement gradually becomes less significant. Particularly, for the cases of *p*=150kPa and 200kPa, the turning points from which the horizontal deformation sharply decreases are *a*/*H*=0.7 and *a*/*H*=0.9 respectively. Besides, after a/H value becomes larger than 0.4 and 0.7 respectively for the cases of *p*=50kPa and 100kPa, the horizontal deformation decreases slowly.

The failure surfaces of the retaining wall and the backfill with different *a*/*H* values are shown in *Figure 4*, from which it can be seen that when the value of *a*/*H* is small, the location where the sliding surface intersects with the wall back is relatively high and the distance between the top of the sliding surface and the wall is relatively small, indicating that the size of the sliding wedge is small. However, with the increase of *a*/*H*, the location where the sliding surface intersects with the wall back gradually descends and the distance between the top of the sliding surface and the wall gradually increases, leading to the enlargement of the size of the sliding wedge. Nevertheless, it is very interesting to note that after *a*/*H* increases to a certain value, the size of the sliding wedge does not increase any more. On the contrary, it begins to decrease and maintain almost a constant value with the continuing increase of *a*/*H*. The turning points for the case of *p*=50kPa, 100kPa, 150kPa and 200kPa are *a*/*H*=0.7, 0.9, 1.1 and 1.3 respectively. After *a*/*H* value becomes larger than that of the turning point, the surcharge has little influence on the failure surface of the geocell reinforced retaining wall and the failure surface becomes the same one with that of the wall without surcharge acting on.

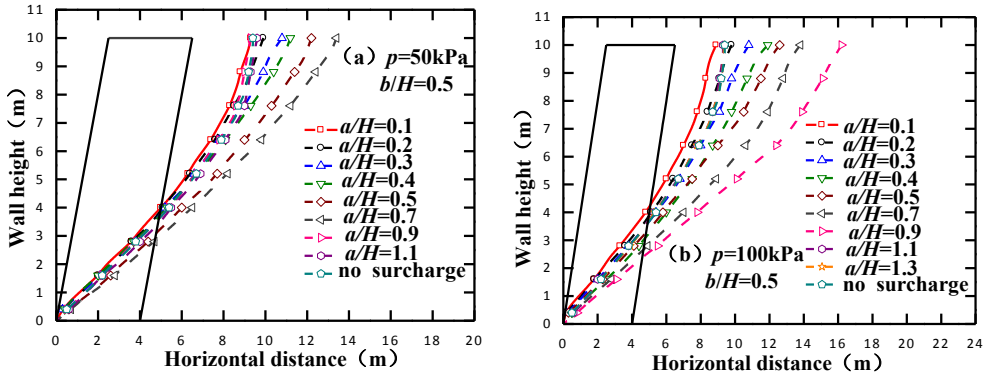

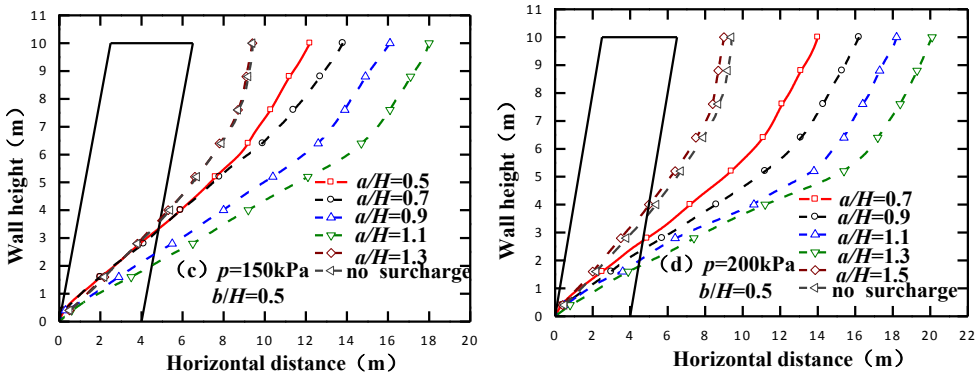

Figure 4 - Effect of distance of surcharge from wall face on the sliding surface (Unit: m)

The variation of the safety factor with *a*/*H* values is illustrated in *Figure 5*. It can be known that the safety factor of the wall without surcharge acting on is 1.423 by computation. It can be observed from *Figure 5* that the safety factor increases with *a*/*H* value. However, after *a*/*H* increases to a certain value, about 0.5*H*, 0.9*H*, 1.1*H* and 1.3*H* for the cases of *p*=50kPa, 100kPa, 150kPa and 200kPa respectively, the safety factor maintains a constant value which is about the same one with that of the wall without surcharge acting on, showing that the effect of surcharge on the safety factor becomes small after *a*/*H* value increases to the one larger than that of the turning point.

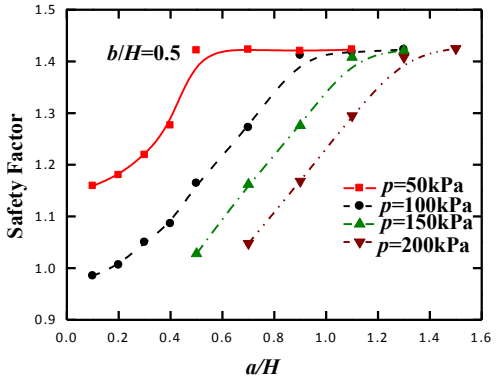

Figure 5 - Effect of distance of surcharge from wall face on the safety factor

Effect of length of surcharge

The effect of the length of the surcharge on the horizontal deformation, the sliding surface and the safety factor are also computed and analyzed by employing the geotechnical finite element method software Plaxis and *p*=100kPa in the computation. The deformation of the wall back with *b*/*H*=0.5, 1, 1.5, and 2 for different *a*/*H* values are shown in *Figure 6*, from which it can be seen that the horizontal deformation of the wall back is relatively small with small *b*/*H* values and it gradually increases with the increase of *b*/*H*. However, after the *b*/*H* value increases to be larger than a certain value, about 1.0 for the cases of *a*/*H*=0.2, 0.5 and 0.8, the horizontal deformation changes very little. For the case of *a*/*H*=0.2, with the increase of the length of the surcharge, the location where the maximum deformation of wall back occurs gradually rises to the middle part of the wall. The maximum deformation of the middle part of the wall is much larger than the other part of the wall, resulting in an acute angle in the middle part of the deflection curve.

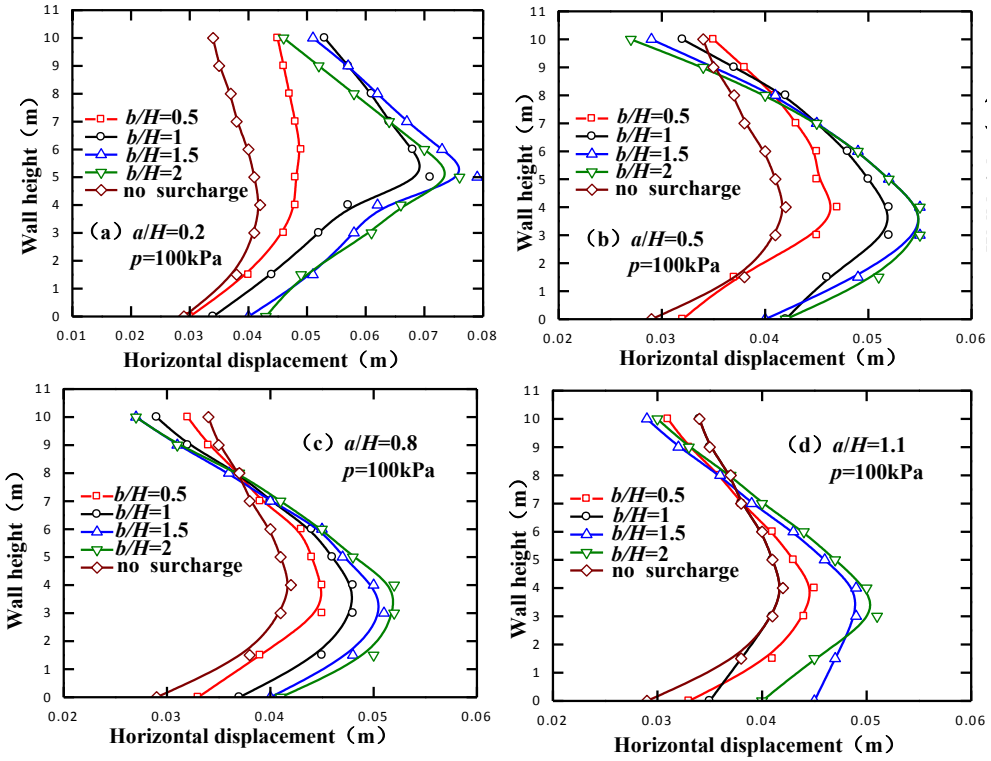

Figure 6 - Effect of length of surcharge on the horizontal deformation (Unit: m)

The sliding surfaces of the wall and the backfill with *b*/*H*=0.5, 1, 1.5 and 2 for different *a*/*H* values are provided in *Figure 7*, from which it can be observed that the sliding surfaces with different *b*/*H* values are almost the same one, indicating that the effect of the length of the surcharge on the sliding surface is not obvious. When *a*/*H* is small, the sliding surface is almost the same one with the wall without surcharge acting on. With the increase of the value of *a*/*H*, the size of the sliding wedge gradually increases. However, when *a*/*H* increases to be larger than 1.1, the size of the sliding wedge reduces to be the one with the wall without surcharge acting on, which has been discussed previously concerning the influences of the distance of the surcharge from the wall face.

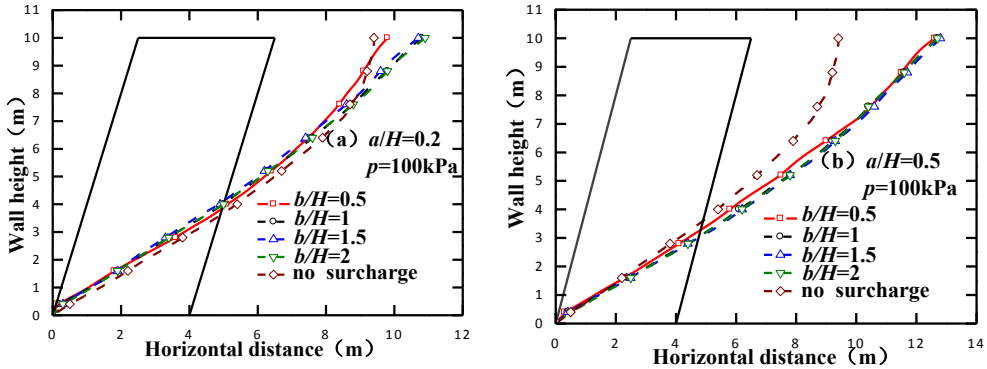

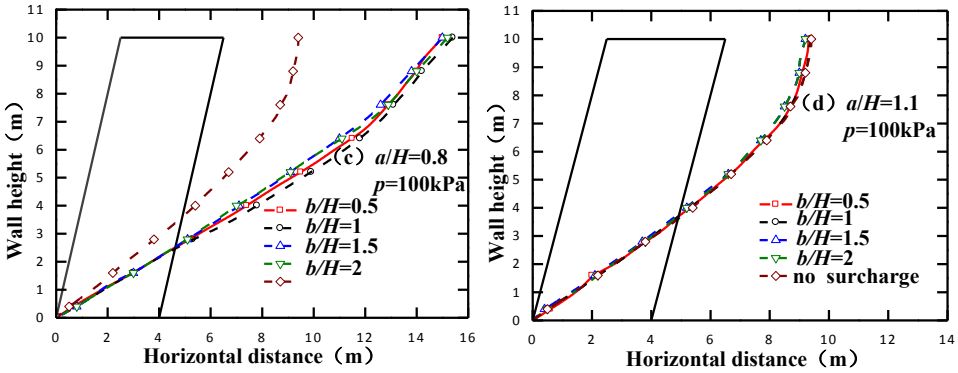

Figure 7 - Effect of length of surcharge on the sliding surface

Safety factors of the wall with *b*/*H*=0.5, 1, 1.5 and 2 for different a/H values are computed by phi-c reduction method and shown in *Figure 8*. It can be observed from *Figure 8* that the safety factor of the wall is large with small *b*/*H* values. However, it gradually decreases with the increase of the value of *b*/*H*. Nevertheless, with the increase of *a*/*H*, the influence of the length of the surcharge on the safety factor gradually becomes small. For example, when *a*/*H*=1.1, the length of the surcharge has no effects on the safety factor of the wall, which does not vary with the value of *b*/*H* and remains the same value with that of the wall without surcharge acting on.

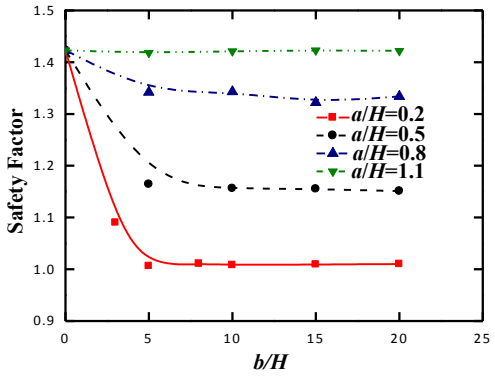

Figure 8 - Variation of Safety factors of the wall with b/H values

CONCLUSION

In this paper, the effect of the distance of the surcharge from the wall face and the length of the surcharge on the horizontal deformation, the failure surface and the factor of safety is studied by employing the geotechnical finite element method software Plaxis. The following conclusions can be primarily drawn on the basis of the analysis of the numerical simulation results.

(1) When the distance of the surcharge from the wall face is small, the horizontal deformation of the wall back is large. When the surcharge moves away from the wall face, the horizontal displacement gradually decreases and the shape of the curve representing the horizontal deformation of the wall back becomes the same one of the wall without surcharge acting on.

(2) When the distance of the surcharge from the wall face is small, the size of the sliding wedge is small. However, with the increase of the distance of the surcharge from the wall face, the size of the sliding wedge gradually increases. Nevertheless, after *a*/*H* increases to a certain value, the

size of the sliding wedge does not increase any more. On the contrary, it begins to decrease with the continuing increase of *a*/*H* and maintain almost a constant value almost the same with that of the wall without surcharge acting on.

(3) The factor of safety increases with the distance of the surcharge from the wall face. However, after a/H increases to a certain value, the safety factor maintains a constant value which is about the same one with that of the wall without surcharge acting on, showing that the effect of the surcharge on the safety factor becomes small in this case.

(4) The horizontal deformation of the wall back is relatively small when the length of the surcharge is small and it gradually increases with the increase of *b*/*H*. However, after the *b*/*H* value increases to be larger than a certain value, the horizontal deformation changes very little.

(5) The effect of the length of the surcharge on the sliding surface is not significant. Besides, the safety factor of the wall gradually decreases with the increase of the length of the surcharge. However, with the increase of a/H, the influence of the length of the surcharge on the safety factor gradually becomes small and after a/H becomes larger than a certain value, the length of the surcharge will have no effect on the safety factor.

ACKNOWLEDGEMENTS

The authors wish to express their sincere gratitude to the Key Industrial Science and Technology Project of Shaanxi Province (No. 2015GY149) and the Scientific Project funded by the Ministry of Housing and Urban-Rural Development of the People's Republic of China Council (No. 2015-K2-008).

REFERENCES

[1] Zigler R., Pokorny M., 2015. Fire protection of timber structures strengthened with FRP materials. Civil Engineering Journal, 4: 1-8.

[2] Liu J., 2016. Design method of bending capacity of continuous composite slab. Civil Engineering Journal, 1: 1-9.

[3] Leshchinsky D., 1989. On the Design of Geosynthetic-Reinforced Walls. Geotextiles and Geomembranes, 8(4): 311-323.

[4] Wong K.S., Broms B.B. , 1994. Failure Modes at model tests of a geotextile reinforced wall. Geotextiles and Geomembranes, 13(6): 475-493.

[5] Porbaha A., Goodings D.J., 1996. Centrifuge modeling of geotextile-reinforced cohesive soil retaining walls. Journal of Geotechnical Engineering, 122(10): 840-848.

[6] Rowe R.K., Skinner G.D., 2001. Numerical analysis of geosynthetic reinforced retaining wall constructed on a layered soil foundation. Geotextiles and Geomembranes, 19: 387-412.

[7] Koerner R.M., Soong T.Y., 2001. Geosynthetic reinforced segmental retaining walls. Geotextiles and Geomembranes, 19(6): 359-386.

[8] Yoo C., 2004. Performance of a 6-year-old geosynthetic-reinforced segmental retaining wall. Geotextiles and Geomembranes, 22(5): 377-397.

[9] Hatami K., Bathurst R.J., 2005. Development and verification of a numerical model for the analysis of geosynthetic-reinforced soil segmental walls under working stress conditions. Canadian Geotechnical Journal, 42(4): 1066-1085.

[10] Bathurst R.J., Vlachopoulos N., Waiters D.L., Burgess P.G., Allen T.M., 2006. The influence of facing stiffness on the performance of two geosynthetic reinforced soil retaining walls. Canadian Geotechnical Journal, 43(12): 1225-1237.

[11] Benjamim C.V.S., Bueno B.S., Zornberg J.G., 2007. Field monitoring evaluation of geotextile-reinforced soil-retaining walls. Geosynthetics International, 14(2): 100-118.

[12] Won M.S., Kim Y.S., 2007. Internal deformation behavior of geosynthetic-reinforced soil walls. Geotextiles and Geomembranes, 25(1): 10-22.

[13] Sabermahani A., Ghalandarzadeh A., Falkher A., 2009. Experimental study on seismic deformation modes of reinforced-soil walls. Geotextiles and Geomembranes, 27(2): 121-136.

[14] Bathurst R.J., Nernheim A., Walters D.L., Allen T.M., Burgess P., Saunders D.D., 2009. Influence of reinforcement stiffness and compaction on the performance of four geosynthetic-reinforced soil walls. Geosynthetics International, 16(1): 43-59.

[15] Leshchinsky D., 2009. On global equilibrium in design of geosynthetic reinforced walls. Journal of Geotechnical and Geoenvironmental Engineering, 135(3): 309-315.

[16] Ehrlich M., Mirmoradi S.H., Saramago R.P., 2012. Evaluation of the effect of compaction on the behavior of geosynthetic-reinforced soil walls. Geotextiles and Geomembranes, 34: 108-115.

[17] Sksiripattanapong C., Chinkulkijniwat A., Horpibulsuk S., Rujikiatkamjorn C., Tanhsutthinon T., 2012. Numerical analysis of bearing reinforcement earth (BRE) wall. Geotextiles and Geomembranes, 32: 28-37.

[18] Liu H.B., 2012. Long-term lateral displacement of geosynthetic-reinforced soil segmental retaining walls. Geotextiles and Geomembranes, 32: 18-27.

[19] Xie Y.L., Yang X.H., 2009. Characteristics of a new-type geocell flexible retaining wall. Journal of Materials in Civil Engineering, ASCE, 21(4): 171-175.

[20] Chen R.H., Chiu Y.M., 2008. Model tests of geocell retaining structures. Geotextiles and Geomembranes, 26(1): 56-70.

[21] Song F., Xu W.Q., Zhang L.Y., Peng Y.G., 2011. Numerical analysis of deformation behavior of geocell flexible retaining wall. Rock and Soil Mechanics, 32(supp.1): 738-742.

[22] Chen R.H., Wu C.P., Huang F.C., Shen C.W., 2013. Numerical analysis of geocell-reinforced retaining structures. Geotextiles and Geomembranes, 39: 51-62.

[23] Song F., Xie Y.L., Yang X.H., Zhang L.Y., 2013a. Failure mode of geocell flexible retaining wall with surcharge acting on backfill surface. Chinese Journal of Geotechnical Engineering, 35(supp.1): 152-155.

[24] Song F., Cao G.R., Zhang L.Y., Tan X.M., 2013b. Numerical analysis of failure mode of geocell flexible retaining Wall. ASCE Geotechnical Special Publication, 232: 136-145.

[25] Song F., Yong L.X., Yang Y.F., Yang X.H., 2014a. Analysis of failure of flexible geocell-reinforced retaining walls in the centrifuge. Geosynthetics International, 21(6): 342-351.

[26] Song F., Li Y. L., Zhang K., Zhang L. Y., 2014b. Study on the optimum sectional form of geocell reinforced retaining wall. // International Journal of Earth Sciences and Engineering, 7, 2, pp. 571-577.

[27] Mhaiskar S.Y., Mandal J.N., 1996. Investigations on soft clay subgrade strengthening using geocells. Construction and Building Materials, 10(4): 281-286.

[28] Bathurst R.J., Knight M.A., 1998. Analysis of Geocell Reinforced-Soil Covers over Large Span Conduits. Computers and Geotechnics, 22(3/4): 205-219.

[29] Latha G.M., 2000. Investigations on the Behavior of Geocell Supported Embankments. Ph.D. thesis, Indian Institute of Technology Madras, Chennai, India.

[30] Rajagopal K., Krishnaswamy N.R., Latha G.M., 2001. Finite element analysis of mbankments supported on geocell layer using composite model. In: Desai, C.S. (Ed). Computer Methods and Advances in Geomechanics. Balkema, Rotterdam, the Netherlands, 1251-1254.

[31] Latha G.M., Rajagopal K., Krishnaswamy IV.R. 2006. Experimental and theoretical investigations on geocell supported embankments. International Journal of Geomechanics, 6(1): 30-35.

[32] Latha G.M., Rajagopal K., 2007. Parametric finite element analyses of geocell-supported embankment.// Canadian Geotechnical Journal, 44, 8, pp. 917-927.

[33] Latha G.M., Dash S.K., Rajagopal K., 2008. Equivalent continuum simulations of geocell reinforced sand beds supporting strip footings. Geotechnical and Geological Engineering, 26: 387-398.

[34] Latha G.M., Dash S.K., Rajagopal K., 2009. Numerical simulation of the behavior of geocell reinforced sand in foundations. International Journal of Geomechanics, 9(4): 143-152.

[35] Mehdipour I., Ghazavi M., Moayed R.Z., 2013. Numerical study on stability analysis of geocell reinforced slopes by considering the bending effect. Geotextiles and Geomembranes, 37: 23-34.

[36] Brinkgreve R.B.J., Broere W., 2000. PLAXIS 2D Version 9 Reference Manual. PLAXIS bv P.O. Box 572.2600 AN DELFT Netherlands.

[37] Wang L.P., 2004. Simulation analysis of engineering behavior of geocell flexible retaining wall. M. Eng. Thesis, Geotechnical and Tunneling Department, School of Highway, Chang'an University, Xi'an, China.

[38] Yang X.H., 2005. Study on engineering character and applied technique of geocell. Ph.D. Thesis, Geotechnical and Tunneling Department, School of Highway, Chang'an University, Xi'an, China.